REVIEW

Chinese Journal of Structural Chemistry

Research Advances of Ferroelectric Semiconductors of 2D Hybrid Perovskites toward Photoelectronic Applications

Yaoyao Chen[1,2†], Changhao Gao[1,2†], Tian Yang[1,2], Wenjing Li[1,3], Haojie Xu[1,3] and Zhihua Sun[1,2,3*]

[1]*State Key Laboratory of Structural Chemistry, Fujian Institute of Research on the Structure of Matter, Chinese Academy of Sciences, Fuzhou 350002, China*

[2]*College of Chemistry, Fuzhou University, Fuzhou 350108, China*

[3]*University of Chinese Academy of Sciences, Beijing 100049, China*

ABSTRACT Ferroelectric materials, characterized by the switchable spontaneous polarization (P_s) through reversing the directions of external electric field, exhibit versatile physical attributes that have been extensively used for practical device applications. Two-dimensional (2D) organic-inorganic hybrid perovskites are recently emerging as a robust family of candidate ferroelectrics, termed ferroelectric semiconductors. In particular, the coexistence and/or coupling of ferroelectric polarization with their semiconducting properties enables new physical concepts, thus providing a potential platform for the development of new multifunctional optoelectronic devices. This review primarily describes the structural origin of symmetry breaking for generating ferroelectric orders in 2D hybrid perovskites, and then presents the combination of ferroelectric P_s with other semiconducting optoelectronic activities. Regarding the emergence of new photoelectric behaviors, the prospects for this 2D family of ferroelectric semiconductors are further discussed, along with their development tendency for the future photoelectronic device applications.

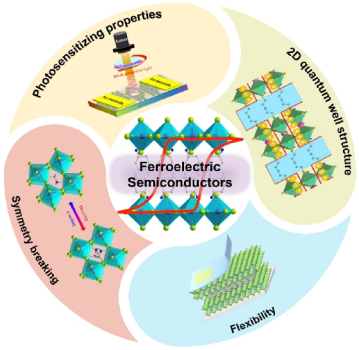

Keywords: ferroelectric materials, hybrid perovskites, semiconductor properties, two-dimensional

n INTRODUNTION

Ferroelectric materials are a typical class of polar crystalline compounds with two or more possible directions of spontaneous polarization (P_s), which can be reversed or changed under the action of the external electric field.[1] The presence of ferroelectric P_s enables abundant macroscopic physical properties, such as dielectric response, piezoelectricity, pyroelectricity, second-order optical nonlinearity, photorefractive effect, *etc*.[2-6] All these attributes have been widely employed for practical device applications, including capacitors, random access memories, infrared detectors, piezoelectric sensors, nonlinear optical devices, and so forth. From the perspective of crystallography, the crystal structures of ferroelectric materials should belong to one of ten polar point groups: C_1 (1), C_s (*m*), C_2 (2), C_{2v} (*mm*2), C_3 (3), C_{3v} (3*m*), C_4 (4), C_{4v} (4*mm*), C_6 (6) and C_{6v} (6*mm*). Especially, the ferroelectric order of crystalline materials usually exists only in a certain temperature range. That is, the emergence of ferroelectric P_s closely relates to the paraelectric-ferroelectric structural phase transition with a critical temperature (the Curie temperature, T_c).[7,8] When the temperature reaches T_c, the compounds undergo very subtle structure changes from a low-symmetric ferroelectric phase (FEP, $T < T_c$) to a high-symmetric paraelectric phase (PEP, $T > T_c$), accompanying with remarkable anomalies of macroscopic physical properties.[9-11] This symmetry breaking is an indispensable indicator for almost all the ferroelectric materials, except for a few cases.[9-11] Consequently, a deep understanding of the relationship between symmetry breaking and ferroelectricity is quite essential for exploring new ferroelectric families and thereby extending their potential device application.[12]

Rochelle salt ($NaKC_4H_4O_6{\cdot}4H_2O$, sodium potassium tartrate tetrahydrate) is the first molecule-based compound that shows intriguing dielectric properties, defining the concept of ferroelectricity analogous to the ferromagnetism.[13] Although its ferroelectric properties and structural phase transition were verified experimentally,[14] the structural complexity and instability still caused difficulties in the early studies on the origin of its ferroelectric orders. Subsequently, the family of ABX_3-type perovskite oxides gradually became the mainstream of ferroelectric portfolios, such as $BaTiO_3$, $Pb(Zr,Ti)O_3$ and $LiNbO_3$, which have greatly promoted the practical device applications of ferroelectric materials. In term of chemical compositions and crystal structures, the ferroelectric compounds have covered a wide range of inorganic oxides, organic compounds, organic-inorganic hybrids, polymers, and liquid crystals. More recently, with the increasing concerns on environmental and sustainable development, molecular ferroelectrics have attracted renewed interest due to their intriguing characteristics of facile preparation, low cost, environmental friendliness, strong compatibility, *etc*. In 2013, Xiong *et al*.[15] reported a molecule-based binary salt of diisopropylammonium bromide, showing the high T_c and large P_s comparable with that of inorganic oxide counterparts, which greatly accelerates the progress of molecular ferroelectrics toward potential applications. Since then, substantial new types of molecular ferroelectrics with fascinating properties have been synthesized and reported, such as metal-free 3D perovskite ferroelectrics[16,17] and organic-inorganic hybrid perovskite ferroelectrics.[18-21]

According to the microscopic mechanisms of symmetry breaking, the ferroelectric phase transitions could be roughly divided into the displacive type and order-disorder type (Scheme 1).

DOI: 10.14102/j.cnki.0254-5861.2022-0013

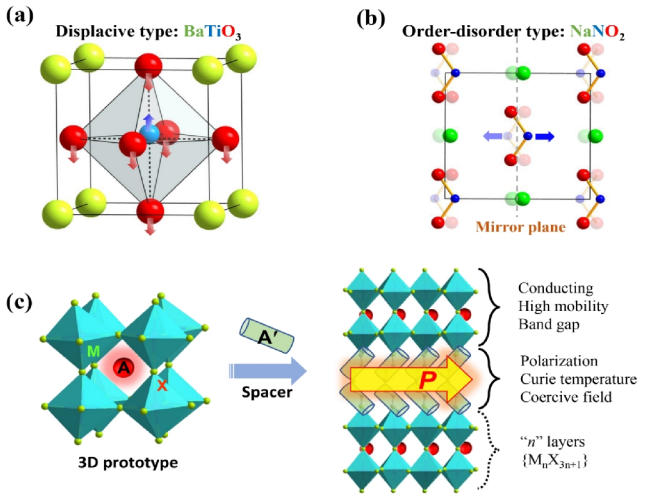

Scheme 1. Schematic illustration of the microscopic mechanism for generating ferroelectric P_s during (a) displacive type and (b) order-disorder type phase transitions. (c) Design strategy for assembling ferroelectric semiconductors in the family of 2D organic-inorganic hybrid perovskites.

Among them, the most of inorganic oxides, such as $BaTiO_3$, $LiNbO_3$, $PbTiO_3$, belong to the displacive type, of which the off-centered displacements of the ions give rise to the spontaneous electric polarization.[22-24] The typical representative of order-disorder type ferroelectrics is $NaNO_2$, of which the dynamic reorientation of electric dipoles about the mirror plane accounts for PEP-FEP phase transition.[25] In reality, these two types of structural phase transitions are not mutually exclusive.[26] As an important branch of molecule-based ferroelectrics, organic-inorganic hybrid perovskites (OIHPs), in which the order-disorder characteristics of organic cations often afford a driving force to the trigger phase transition,[27-29] have recently attracted renewed attentions on account of their infinite structural flexibility and processability. In particular, the 2D family of OIHPs, combining ferroelectric orders with their unique semiconducting merits, would behave as a potential candidate for fabricating the newly-conceptual photoelectronic devices.[30,31] Up to date, the most well-developed subclass of 2D OIHPs is the Ruddlesden-Popper (RP) structure, which adopts a general chemical formula of $(A')_2(A)_{n-1}M_nX_{3n+1}$,[32] where A' denotes organic spacer, A is perovskitizer, M is divalent metal and X is anion. The *n* value presents the number of inorganic perovskite layers (Scheme 1c). From a structural design viewpoint, such multilayered architectures can be established by the chemical alloying of mixed-organic cations (A and A'), for which the strong structural compatibility allows diverse physical properties.[33,34] In the 2D family of OIHPs, the organic sheets and inorganic sheets are arranged alternately to constitute the quantum-confined structure, of which the perovskite components make a crucial role for their semiconducting properties, such as optical bandgap and electrical conductivity. Meanwhile, the organic spacing cations allow molecular freedom of dynamic motions to trigger phase transitions and ferroelectric spontaneous polarization. These structural characteristics of 2D OIHPs thus endow the combination of semiconducting electric conductivity and ferroelectricity. Most interestingly, the subtle chemical modification not only results in the targeted compounds but also optimizes their physical properties. The main design strategies include tailoring the A/A'-site organic cations, modifying inorganic perovskite frameworks, and regulating the number of inorganic layers (*i.e.*, *n* value); all these methods have been utilized to realize the rational design of new multifunctional ferroelectric materials.[35-37] In this review, we have summarized the recent advances of 2D OIHP-type ferroelectrics materials, termed ferroelectrics semiconductors. Primarily, the structural changes of symmetry breaking for generating ferroelectric orders are analyzed. The combination and/or coupling of ferroelectric P_s with other semiconducting activities results in new optoelectronic behaviors. Furthermore, the prospects of these 2D ferroelectric semiconductors are also discussed, as well as their future development trend for photoelectronic device applications.

n PEROVSKITE-TYPE MONOLAYERED FERROELECTRIC SEMICONDUCTORS (*n* = 1)

Perovskite-type structures are generally defined by a framework of corner-sharing MX_6 octahedra. This concept refers to the mineral $CaTiO_3$ that comprises the 3D anionic network with Ca^{2+} cations locating inside the space formed by corner-sharing TiO_8 octahedra. As the low-dimensional subclass, the 2D layered hybrid perovskites can be formed by the conceptual slicing of a 3D prototype lattice along with a certain index (Scheme 1c). For instance, the majority of 2D RP-type structures are the <100>-oriented perovskites with the cutting planes perpendicular to crystallographic <100> direction. In terms of the thickness of inorganic sheets, the monolayered perovskites (*n* = 1) belong to the simplest 2D structure of $(A')_2(A)_{n-1}M_nX_{3n+1}$ family. There is only one type of organic cation (A') serving as the spacing moiety, which is alternatively arranged with the perovskite sheets. Owing to the remarkable structural flexibility, the monolayered hybrid perovskites allow the incorporation of versatile organic cations, of which the dynamic motions and reorientations give rise to their ferroelectric orders.

(n-BA)$_2$PbCl$_4$ (Compound 1). Basic crystal structure of **1** consists of the infinite layers of corner-sharing $PbCl_6$ octahedra separated by the bilayers of organic *n*-butylammonium (*n*-BA) cations. At room temperature, all the organic cations are orderly arranged along the *c*-axis, which also indicates the direction of P_s at FEP (Figure 1a).[38] With the temperature increasing, the *n*-BA^+ cations become disordered and create the crystallographic *m* mirror plane at high-temperature PEP. Symmetry breaking with an Aizu notation *mmm*F*mm*2 was solidly verified, showing the transformation from centrosymmetric space group *Cmca* (E, C_2, $2C_2'$, i, σ_h, $2\sigma_v$) to the polar one $Cmc2_1$ (E, C_2, $2\sigma_v$) at FEP. This process belongs to one of the 88 phase transitions for ferroelectric materials. Intuitively, the evidence for ferroelectricity, *i.e.*, electric polarization *versus* electric field (*P*-*E*) hysteresis loop, was measured along the crystallographic c^{FEP}-axis (Figure 1b). The saturated P_s of 2.1 $\mu C \cdot cm^{-2}$ and coercive force field (E_c) of 14.3 $kV \cdot cm^{-1}$ were obtained at 300 K, falling in the range of other analogue ferroelectrics of OIHPs.

Interestingly, the structural distortion of $PbCl_6$ octahedra of this

DOI: 10.14102/j.cnki.0254-5861.2022-0013

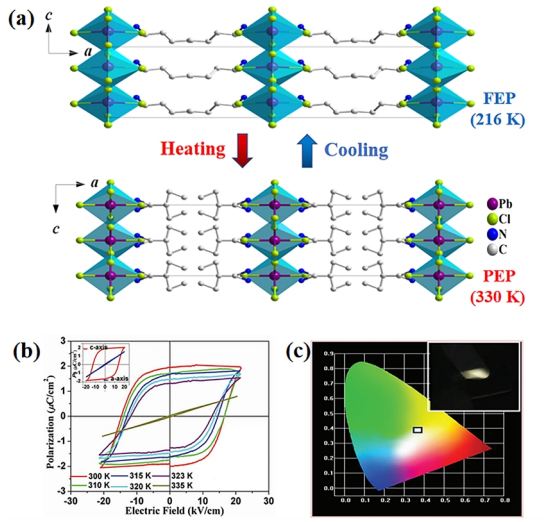

Figure 1. (a) Project of crystal structures of **1** at FEP (216 K) and PEP (330 K). (b) *P-E* hysteresis loops measured along the c^{FEP}-axis direction. Inset: *P-E* hysteresis loops collected along the a^{FEP}- and c^{FEP}-axis directions. (c) CIE chromaticity coordinates of **1** in the color space chromaticity diagram. Inserted: the white light emission picture excited at 336 nm.

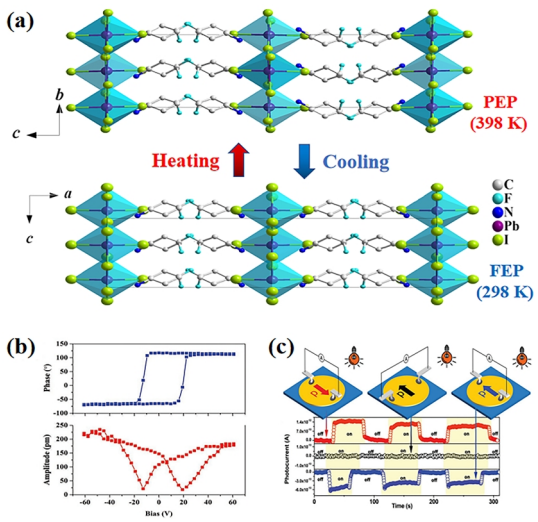

Figure 2. (a) Packing structures of **2** collected at PEP (398 K) and FEP (298 K), projected along the *a*- and *b*-axis, respectively. Hydrogen atoms are omitted for clarity. (b) Local lateral PFM switching spectroscopy. (c) Schematic diagram of FEPV measurement with the electrodes aligned parallel and perpendicular to the P_S direction. Short-circuit photocurrent in the different experimental setup (indicated by different colors), respectively.

OIHP not only contributes to excellent ferroelectricity, but also contributes to the broadband spectral emission.[39] When subjected to 336 nm excitation, **1** exhibits a wide spectral range of white emission covering the whole visible region with a maximum at 543 nm. As shown in Figure 1c, the emission locates near the yellow side of pure white light with the Commission Internationale de L'Eclairage (CIE) chromaticity coordinate of (0.37,0.40) and a correlated color temperature of 4423 K corresponding to the "warm" white light, which is advantageous for solid-state lighting and display applications. In addition, the broadband emission of **1** also affords excellent color rendition with high color rendering index (CRI) up to ≈ 86. This value is even higher than the typical fluorescent light source (CRI ≈ 65). The photoluminescence (PL) quantum efficiency (1%) and lifetime (τ_1 ≈ 2.59 ns, τ_2 ≈ 9.68 ns) were also measured for this white-light luminescent ferroelectric. As far as we are aware, the combination of ferroelectricity and broadband white-light emission in the single-phase material might open up a potential pathway toward the integrated optoelectronic devices.

$(DFCHA)_2PbI_4$ (Compound 2). Compared with lead-chloride counterparts, the lead-iodide hybrid perovskites have shown remarkable advantages of optical absorption and electrical transport properties. To explore ferroelectric semiconductors of lead-iodide family, the method of fluorine modification was used to design organic spacing cations, of which the dynamic motions allow for ferroelectric orders, as verified in compound $(DFCHA)_2PbI_4$ (where DFCHA is 4,4-difluorocyclohexylammonium).[40] Thermal analyses reveal that **2** undergoes a structural phase transition at 377 K (T_c). At the PEP (above T_c), it features a 2D RP-type perovskite structure with the non-polar centrosymmetric space group of *Pbca*. The 2D inorganic perovskite sheets consist of infinite corner-sharing PbI_6 octahedra, and two layers of organic DFCHA cations occupy the space between adjacent sheets (up, Figure 2a). It is noteworthy that in the unit cell of PEP, two layers of DFCHA cations are linked to lead-iodide sheets with different orientations, thus cancelling out the net polarization. With temperature decreasing below T_c, **2** crystallizes in the polar space group of $Cmc2_1$ at FEP. Compared to the structure at PEP, all the organic DFCHA cations exhibit the consistent arrangement in the unit cell, and their reorientations break the inversion symmetry. Consequently, the macroscopic polarization could be generated by such an arrangement (down, Figure 2a). This structural change with an Aizu notation of *mmm*F*mm*2 is one of the 88 species of ferroelectric phase transitions.[41,42] The electric switching of P_S verified by lateral piezoresponse force microscopy (PFM) confirms its ferroelectric properties. As shown in Figure 2b, the distinct 180° switching of the PFM phase signals with the hysteresis behavior as well as the butterfly-shaped amplitude signals indicates the switchable electric polarization of **2**.

Structurally, the inorganic lead-iodide frameworks make an important role to the optical and semiconducting properties of **2**. The optical bandgap of ~2.38 eV was obtained from the *Tauc* equation, of which the valence band maximum and conduction band minimum involve with the electronic states of Pb and I atoms that determine its optical bandgap. Furthermore, ferroelectric photovoltaic (FEPV) effects were achieved in the single crystals of **2** (Figure 2c). Crystal-based device with two electrodes parallel to the polarization direction exhibits a photovoltaic short-circuit photocurrent (I_{sc}) with the amplitude of ~1 pA under white light (red curve, Figure 2c). Subsequently, large voltage was applied to reverse polarization direction, and the results clearly show that I_{sc} should stem from the ferroelectric polarization. That is, the FEPV effects in **2** are the main mechanism,

DOI: 10.14102/j.cnki.0254-5861.2022-0013

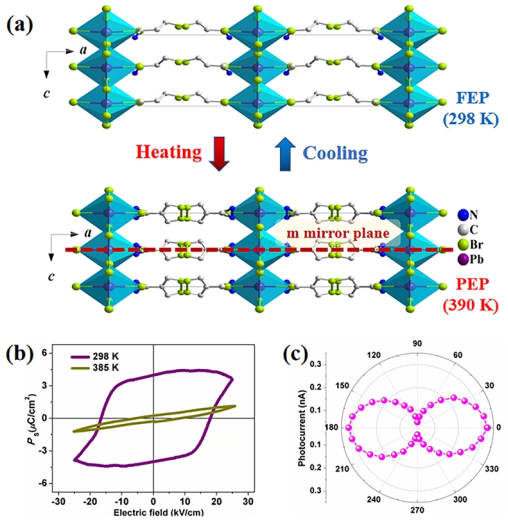

Figure 3. (a) Project of crystal structures of **3** at FEP (298 K) and PEP (390 K). (b) Variable-temperature *P-E* hysteresis loops measured along the c^{FEP}-axis. (c) Plot of the resolved I_{sc} as a function of the polarized-light polarization angles at FEP.

thus eliminating the possibility of potential asymmetry caused by depolarization electric field effect, optical rectification effect and electrode asymmetry. Such findings would highlight the potentials of **2** for perovskite solar cells and other optoelectronic device applications.

$(BPA)_2PbBr_4$ (Compound 3). The modification of organic spacing cations is an effective pathway to trigger ferroelectric orders of the 2D family of hybrid perovskites. Under the guidance of hydrogen/halogen substitution, we have successfully synthesized a new ferroelectric of $(BPA)_2PbBr_4$ (BPA = 3-bromopropylammonium) that adopts the 2D RP-type motif,[43] which consists of the inorganic monolayered perovskite frameworks and interlaced bilayers of organic BPA^+ spacer (Figure 3a). At the room-temperature phase, it is interesting that the organic moieties are fully ordered with the C–N bonds orienting along the *c*-axis. With the temperature increasing above T_c, the inorganic $PbBr_6$ octahedra transform into the symmetric configuration and BPA^+ cations become highly-disordered, locating with respect to the crystallographic *m* mirror plane. This order-disorder phase transition accompanies with the symmetry breaking from a centrosymmetric space group *Cmca* (the point group *mmm*, at PEP) to the polar one $Cmc2_1$ (the point group *mm*2, at FEP), being reminiscent of possible ferroelectricity. Furthermore, the measurements of temperature-dependent *P-E* hysteresis loops verify the ferroelectric properties of **3**. As shown in Figure 3b, the linear trace reveals its paraelectric behavior above T_c, whereas the typical *P-E* hysteresis loops with good rectangularity provide direct evidence for its switchable polarization. At 298 K, the P_s and coercive field (E_c) are about calculated as 4.8 $\mu C \cdot cm^{-2}$ and 18.2 $kV \cdot cm^{-1}$ respectively, which are on the par with other OHIP ferroelectrics.

The strong light-matter interactions in ferroelectric materials lead to new concept of photoelectronic properties. Here, notable FEPV effects were clearly observed in the bulk crystals of **3** under UV illumination with an intensity of 45 $mW \cdot cm^{-2}$, showing the open-circuit photovoltage (V_{oc}) of 0.85 V and I_{sc} of ~0.5 nA, respectively. Such bulk FEPV responses are mainly derived from the electric P_s, which can create a built-in electric field to separate the photogenerated carriers without applying external bias.[44-46] Given the quite low dark current (I_{dark}, 1.2×10^{-14} A), a large ratio of current (I_{sc}/I_{dark}) up to ~10^4 was obtained under the irradiation of 377 nm light. In combination of P_s-induced FEPV effects and natural 2D anisotropy, the new prospects of self-driven polarized-light detection for **3** can be expected. Figure 3c displays the resolved I_{sc} as a function of the polarization angles of polarized-light, giving the maximum polarization ratio (I_{max}/I_{min}) of ~6.8. This figure exceeds some other UV polarized-light sensitive materials, such as ZnO, GaN, GeS_2, *etc*. Besides, the photoresponsivity (R_λ) and detectivity (D^*) of the device were estimated as 10^{-4} A/W and 10^7 Jones (0 V bias, 1.5 $mW \cdot cm^{-2}$). These results indicate that the self-powered photodetectors based on single crystals of **3** have remarkable potentials toward the polarization-sensitive photodetection in the UV region.

n PEROVSKITE-TYPE BILAYERED FERROELECTRIC SEMICONDUCTORS $(A')_2AM_2X_7$ (*n* = 2)

The huge structural flexibility of 2D hybrid perovskites allows for accommodation of diverse ammonium spacing cations, of which a large freedom degree of molecular motions are the key elements to realize ferroelectric properties.[47] Meanwhile, the modification of inorganic networks and regulation of layer numbers (*i.e.*, *n* value) are feasible to improve their semiconducting properties. Particularly, the 2D multilayered RP-type hybrid perovskites $(A')_2(A)_{n-1}M_nX_{3n+1}$ combine the different properties of organic and inorganic components in a single-molecule complex, acting as an ideal platform to expand new physical concepts. For ferroelectric semiconductors, however, a subtle balance should be taken between ferroelectricity and conductivity, because the severe P_s deterioration might be caused by the leakage current of photoexcited carriers. In this section, we will mainly highlight the typical examples of ferroelectric semiconductors of $n > 1$ multilayered hybrid perovskites.

The photo-induced properties that coexist and/or combine with ferroelectric P_s include two-photon nonlinear optical absorption, polarized-light sensitivity, X-ray detection, self-driven photodetection, *etc*.

(n-BA)$_2$(FA)Pb_2Br_7 (Compound 4). The <100>-oriented bilayered perovskites (n = 2) are the main members that have been crystallographically characterized, and compound **4** is selected as one of the representative cases of this series. It crystallizes in the polar space group $Cmc2_1$ and adopts a typical bilayered perovskite motif. As shown in Figure 4a, its ferroelectric structure consists of bilayers $[Pb_2Br_7]_\infty$ stacked along the *a*-axis,[48] and the organic *n*-BA^+ cations are distributed between the adjacent $[Pb_2Br_7]_\infty$ sheets. The small-size FA^+ cations (FA = formamidine) are confined inside the central cavity formed by the $PbBr_6$ corner-sharing octahedra. The dynamic orderings of or

DOI: 10.14102/j.cnki.0254-5861.2022-0013

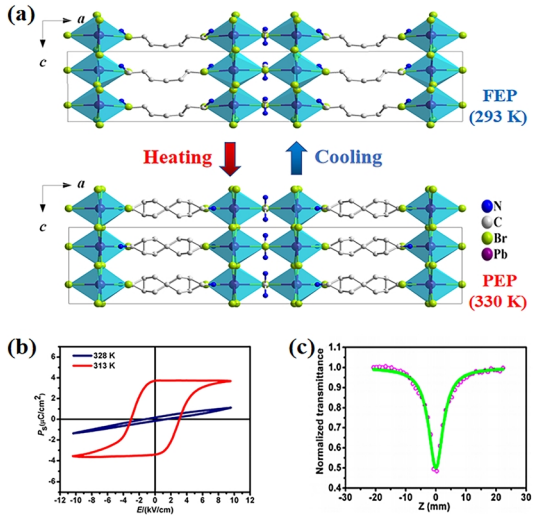

Figure 4. (a) Packing structures of **4** viewed along the *b*-axis direction at FEP (293 K) and PEP (330 K). (b) The *P*-*E* hysteresis loops measured at different temperatures. (c) Open aperture *Z*-scan experimental responses.

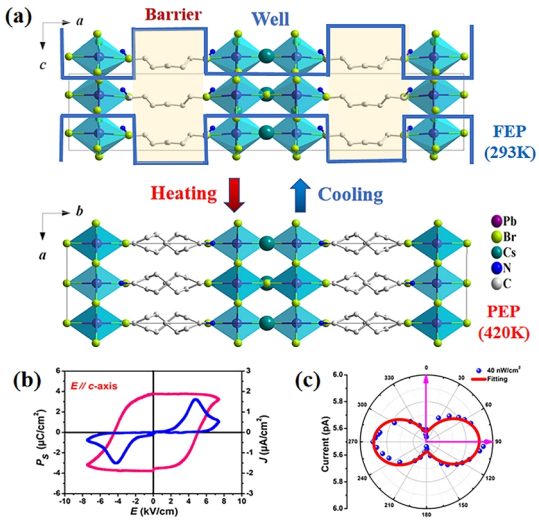

Figure 5. (a) Diagram for the crystal structures of **5** at FEP (293 K) and PEP (420 K). (b) The *P*-*E* hysteresis loop and the corresponding *J*-*E* curve. (c) Polar plot of the normalized angle-resolved photocurrents (λ = 405 nm, 40 nW·cm^{-2}).

ganic *n*-BA$^+$/FA$^+$ cations result in ferroelectric phase transition at 322 K. The alternative stacking of organic and inorganic components resemble the typical 2D quantum-well structure,[49] which would exert significant influences on the two-photon absorption characteristics. With temperature increasing beyond its T_c (~322 K), the paraelectric structure transforms to the centrosymmetric space group *Cmcm*, along with the organic cations becoming disordered. During this phase transition, the crystallographic symmetry elements are halved from 8 (*E*, C_2, $2C_2'$, *i*, σ_h, and $2\sigma_v$) at PEP to 4 (*E*, C_2, and $2\sigma_v$) at FEP, revealing the symmetry breaking with an Aizu notation of *mmm*F*mm*2. The measured *P*-*E* hysteresis loop demonstrates that **4** has the P_s value of ~3.8 μC·cm^{-2} at 313 K, coinciding with the calculated P_s value by the point charge model.

The 2D perovskite frameworks of **4** constructed by alternative arrangement of organic and inorganic components resemble 2D quantum wells, of which inorganic sheets are “wells” and organic bilayers act as “barriers”. This intrinsic quantum-well structure creates interesting quantum and dielectric confinement effects. Photoexcited charge carriers might be strongly confined in inorganic wells to enhance light-matter interactions, thus leading to abundant photoelectronic properties. According to the Z-scan result, the nonlinear optical absorption provides a large two-photon absorption coefficient of ~5.76×10^3 cm·GW^{-1} for **4**. This figure is almost two orders of magnitude larger than that of the inorganic oxide ferroelectrics. Such results highlight the further exploration of new ferroelectric materials of hybrid perovskites toward nonlinear optical applications.

(*n*-BA)$_2$CsPb$_2$Br$_7$ (Compound 5). The inorganic perovskite frameworks are chemically modified to design new ferroelectric semiconductors, (*n*-BA)$_2$CsPb$_2$Br$_7$,[50] of which the corner-sharing PbBr$_6$ octahedra construct the {CsPbBr$_3$}$_n$ sheets with Cs$^+$ cations in the cavities and organic bilayers of *n*-BA$^+$ cations located between adjacent inorganic perovskite sheets (Figure 5a). Compound **5** is a room-temperature ferroelectric that crystallizes in the polar space group $Cmc2_1$. Above the T_c (412 K), its frameworks adopt the symmetric configuration with Cs$^+$ cation occupying the cavity center and organic cations becoming disordered at PEP. The symmetry breaking involves with the disordering of organic cations and displacement of anionic moieties.[51] The curves of *P*-*E* hysteresis loop and current density *versus* electric field (*J*-*E*) confirm that **5** has a large P_s of 4.2 μC·cm^{-2} along the polar *c*-axis direction (Figure 5b).

As expected, the alternative alignment of inorganic and organic layers constructs the 2D Type-I quantum wells. The inorganic sheets of PbBr$_6$ octahedra distribute along the *bc* plane, and the unstable ns^2 lone pairs of Pb^{2+} ions favor mobility of photocarriers that can easily transfer along the *c*-axis direction. In contrast, the carriers must cross the energy barrier along the *a*-axis direction, which is not conducive to the carrier transport. Given the built-in electrostatic field induced by P_s, it is conducive to the separation and transport of carriers along the *c*-axis direction. All these inherent merits of electric and optical anisotropy will benefit the polarized-light detection performances of **5**. As shown in Figure 5c, the dichroic photocurrent results of maximum value (I_{ph}^c) and minimum value (I_{ph}^a) afford the ratio (I_{ph}^c/I_{ph}^a) to be ~1.5, which is comparable to the ratio of other inorganic counterparts. It should be emphasized that even at an incident light power density of ~40 nW·cm^{-2}, this detector shows highly-sensitive responses to the weak po larized-light. As far as we know, this work provides a bright prospect for the effective polarized-light detection using ferroelectric semiconductors.

(HA)$_2$CsPb$_2$Br$_7$ (Compound 6). Basic structural architecture for **6** adopts a 2D Cs-based perovskite topology, in which the inorganic Cs$^+$ cation templates perovskite sheets and the organic HA$^+$ (HA = *n*-hexylammonium) cation behaves as the “spacer”

Chin. J. Struct. Chem. **2022**, 41, 2204001-2204011
DOI: 10.14102/j.cnki.0254-5861.2022-0013

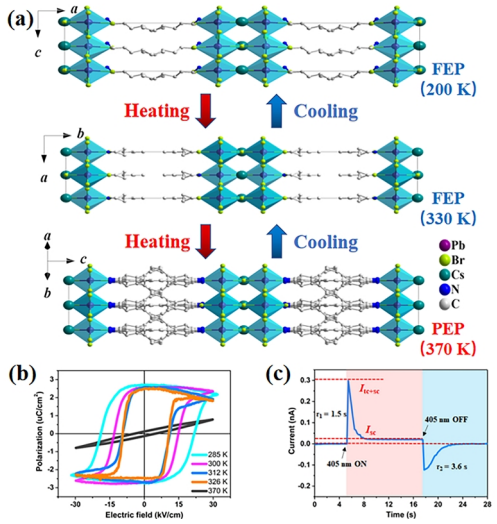

Figure 6. (a) Diagram of packing structures of **6** collected at FEP (200 K) and PEP (370 K). (b) The *P-E* hysteresis loops measured at different temperatures. (c) One cycle of the ferro-pyro-phototronic photocurrent.

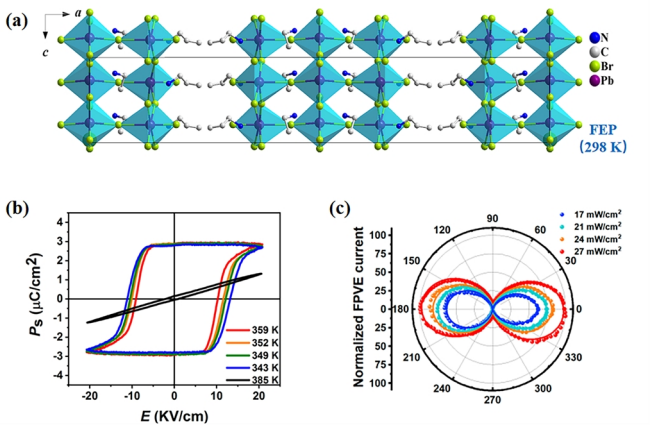

Figure 7. (a) Crystal structure diagram of **7** projected along the *b*-axis at FEP (298 K). (b) The *P-E* hysteresis loops measured along the c^{FEP}-axis at different temperatures. (c) Polar coordinate of FEPV current I_{sc} as a function of polarized-light angle under different light intensities at 298 K.

(Figure 6a). Compared with the typical perovskite motifs containing organic cations as the perovskitizer,[52] electrostatic interactions between $PbBr_6$ octahedra and Cs^+ cations afford great possibilities for the occurrence of atomic displacement. Remarkably, the dynamic motions of Cs^+ cations and tilting of $PbBr_6$ octahedra, along with the frozen ordering of HA^+ cations, trigger multiple phase transitions of **6** around 303 and 349 K. Symmetry breaking occurs with an Aizu notation of 4/*mmm*F*mm*2, as deduced by variable-temperature structure changes from paraelectric space group *I*4/*mmm* to the polar one *Fmm*2 and *Cmc*2_1 at FEP. Ferroelectricity of **6** was further confirmed by the measurement of *P-E* hysteresis loops along the polar *c*-axis (Figure 6b). The *P-E* hysteresis loops keep well-defined rectangular pattern, and the P_s value of 2.5 μC/cm^2 falls in the range of other analogue ferroelectrics.

Considering its temperature-dependent ferroelectric P_s and photosensitive activities caused by inorganic networks, **6** is expected to be a potential candidate that enables the photo-induced pyroelectricity and ferro-pyro-phototronic (FPP) effects.[53] As shown in Figure 6c, exceptionally large FPP effects are observed in **6**, which allow a giant boosting of transient photopyroelectric currents to ~1500% compared with the steady-state photovoltaic signals; this figure-of-merit is superior to the majority of inorganic oxide counterparts. Furthermore, the direction of these FPP effects can be facilely switched and controlled through external electric filed, revealing a crucial role of ferroelectric polarization to this three-channel coupling. The results afford a new avenue to tune physical properties of ferroelectrics and forward their potentials to smart optoelectronic device applications.

n PEROVSKITE-TYPE TRILAYERED FERROELECTRIC SEMICONDUCTORS $(A')_2A_2M_3X_{10}$ (*n* = 3)

In addition to bilayered perovskite series, the <100>-oriented trilayered candidates $(A')_2A_2M_3X_{10}$ (*n* = 3) are also investigated as the potential ferroelectric semiconductors. By increasing the thickness of inorganic sheets, the optical and photoelectric properties can be optimized, which also show potentials for sensitive photodetection[54], polarized-light detection in the solar-blind UV region, multiphoton absorption (MPA), *etc*.

$(ALA)_2(EA)_2Pb_3Br_{10}$ (Compound 7). Bulk FEPV effect represents a typical coupling of ferroelectric P_s with photovoltaic behavior. Recently, the concept of polarized-light detection has been achieved through bulk FEPV effects of a 2D trilayered perovskite ferroelectric, $(ALA)_2(EA)_2Pb_3Br_{10}$ (where ALA is allylammonium and EA is ethylammonium).[55] Structural analyses reveal that **7** has a trilayered perovskite motif with EA^+ cation acting as "perovskitizer" inside the cavity of corner-sharing $PbBr_6$ octahedra, while ALA^+ behaves as "spacer" in the interlayer space of inorganic sheets. At the high-temperature PEP, compound **7** crystallizes in the nonpolar space group *I*4/*mmm* with 16 symmetry elements (E, $2C_4$, C_2, $2C_2'$, $2C_2''$, $2S_4$, i, σ_h, $2\sigma_v$, $2\sigma_d$). With the temperature cooling down, it undergoes two phase transitions and belongs to the polar space group *Cmc*2_1 (E, C_2, $2\sigma_v$) at room-temperature FEP (Figure 7a). The reorientation of organic moieties and distortion of $PbBr_6$ octahedra lead to the separation of positive and negative charge centers, giving rise to the dipole moment (-7.3569×10^{-29} cm) and electric polarization along the *c*-axis. Hence, the symmetry breaking occurs with an Aizu natation of 4/*mmm*F*mm*2, of which the four equivalent directions indicate biaxial ferroelectricity for **7**. The ferroelectricity was proved by temperature-dependent *P-E* hysteresis loops with good rectangularity (Figure 7b).

It is notable that excellent P_s-induced bulk FEPV effects are observed in **7**, including near-bandgap photovoltage of ~2.5 V and large current on/off ratio of ~10^4 under 405 nm irradiation. Figure 7c displays the angle-resolved FEPV I_{sc} curves under different light intensities and the polarization ratio ω_{sc} ($\omega_{sc} = I_{max}/I_{min}$) is as high as ~15. As far as we know, this innovative work on the P_s-induced bulk FEPV effect opens up a new pathway for

DOI: 10.14102/j.cnki.0254-5861.2022-0013

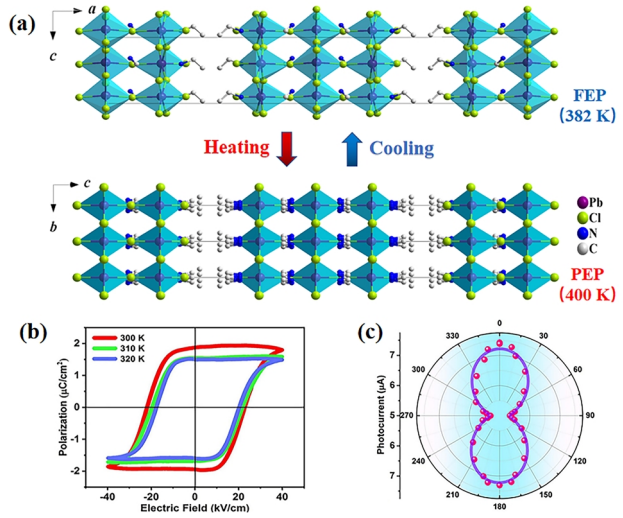

Figure 8. (a) Variable-temperature crystal structures of **8** at FEP (382 K) and PEP (400 K). (b) The *P-E* hysteresis loops measured at different temperatures. (c) Polar coordinate diagram of the angle-resolved photocurrent I_{sc}.

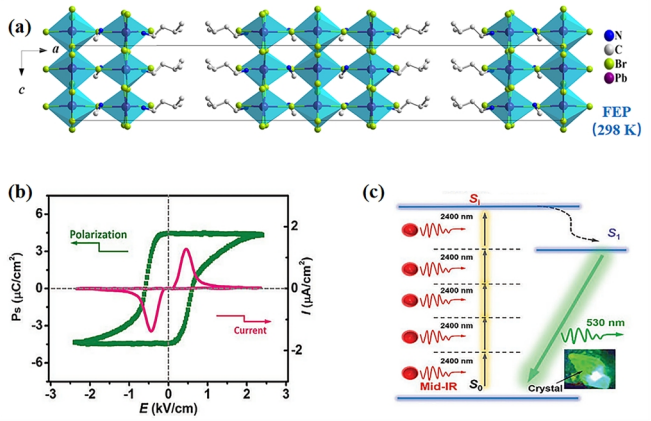

Figure 9. (a) Crystal structure of **9** viewed along *b*-axis at FEP (298 K). It adopts an alternative array of inorganic perovskite sheets and organic cation layers. (b) *P-E* hysteresis loop and *J-E* curve measured at room temperature. (c) Energy diagram and PL picture of the crystal wafer during 5PA process.

sensitively detecting polarized-light detection, and further expands the application of OIHP-type ferroelectric materials in smart optoelectronic devices.

$(EA)_2(MA)_2Pb_3Cl_{10}$ (Compound 8). Through the 3D-to-2D reduction of cubic prototype, we have recently designed the 2D ferroelectric of $(EA)_2(MA)_2Pb_3Cl_{10}$ (**8**),[56] which adopts the trilayered perovskite structure with organic MA^+ cation acting as "perovskite" and EA^+ moiety locating in the space between adjacent inorganic sheets (Figure 8a). The ferroelectric structure of **8** crystallizes in the polar space group *Cmc*2_1. Both organic MA^+ and EA^+ cations are ordered with the NH_3 groups tightly anchored to $PbCl_6$ octahedra by N–H···Cl hydrogen bonds (Figure 8a). The positively charged cations tilt along the *c*-axis, and the distorted $PbCl_6$ octahedra deviate towards the opposite direction, thus leading to the generation of dipole moment and electric polarization. With temperature increasing up to 400 K (PEP), its structure transforms into a non-polar space group *I*4/*mmm*. Both types of organic cations become highly disordered at PEP, corresponding to the phase transition at 390 K (T_c). Ferroelectric properties of **8** are well confirmed by the *P-E* hysteresis loops (Figure 8b), which afford the P_s value of ~1.8 μC·cm^{-2} at room temperature.

With respect to semiconducting properties, compound **8** exhibits a wide bandgap (E_g ~3.35 eV) and anisotropic absorbance caused by its inherent 2D motif. Such attributes are favorable to the polarization-sensitive UV photodetection.[57,58] As expected, the crystal-based devices show excellent polarization-sensitive activities under 266 nm, including large dichroism (~1.38) and high on/off current ratios (~2.3×10^3). Figure 8c shows the polar plot of angle-resolved photocurrents under an external bias voltage (10 V). By controlling polarized-light angle, the photocurrents exhibit significant periodic changes. The maximum value (I_{max}) emerges at 0° and 180° polarization, corresponding to the light polarized along *c*-axis; when the light is polarized parallel to *a*-axis (90° and 270°), the minimum photocurrent (I_{min}) is observed. As the study on the polarization-sensitive UV photodetection, this work provides an effective method for exploring new 2D hybrid perovskite candidate materials for future optoelectronic applications.

$(IA)_2(MA)_2Pb_3Br_{10}$ (Compound 9). Regarding the strong light-matter interactions, multiphoton absorption (MPA) is the nonlinear optical process that has potential applications in optical data storage, optical communication, and biological imaging.[59] We presented the high-order MPA activities in the ferroelectric of $(IA)_2(MA)_2Pb_3Br_{10}$ (**9**),[60] which adopts a 2D trilayered perovskite structure with an alternative array of inorganic perovskite sheets and organic IA^+ layers. Structural analyses reveal that order-disordering of IA^+ and MA^+ cations affords a driving force to trigger their phase transition at T_c = 305 K, and their reorientation and tilting motions result in electric polarization. Above the T_c, compound **9** belongs to the tetragonal system. Both organic IA^+ and MA^+ cations feature the disordered molecular configurations with eight equivalent orientations. In contrast, their crystal structures transform to the orthorhombic system below the T_c. Two types of cations become fully ordered with the protonated NH_3^+ groups connected to $PbBr_6$ octahedra through N–H···Br hydrogen bonds. The results of *P-E* hysteresis loop and *J-E* curve confirm that compound **9** has a large P_s of 5.0 μC·cm^{-2} (Figure 9b), which is on the par with those of other ferroelectrics in hybrid perovskite family.

The unique 2D trilayered perovskite structure of **9** enables strong dielectric and quantum confinement effects on free carriers, which would be potential for exploring high-order MPA properties. Figure 9c shows the energy diagram of the five-photon absorption (5PA) process of **9**. After laser irradiation (≈ 2400 nm), the excitons (*i.e.*, electron-hole pairs) are formed by absorbing five mid-infrared photons at the same time, in which the total energy is sufficient to overcome the energy gap between the ground state (S_0) and excited state (S_i). Subsequently, the interband decay to the lower exciton state (S_1) causes the MPA of about 530 nm to excite PL emission. Here, compound **9** exhibits giant broadband

DOI: 10.14102/j.cnki.0254-5861.2022-0013

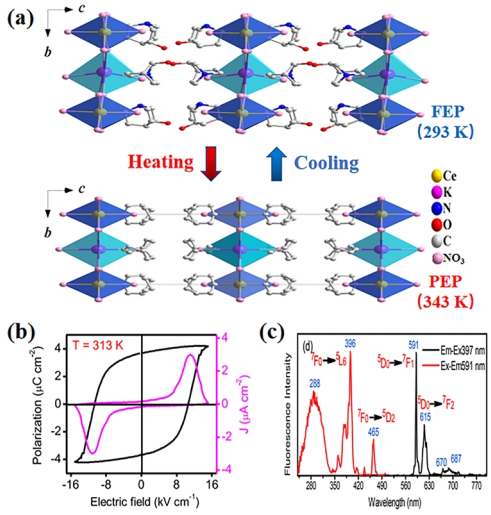

Figure 10. (a) Crystal structures of **10** collected at FEP (293 K) and PEP (343 K). (b) *P-E* hysteresis loops and *J-E* curve measured at 313 K. (c) Emission and excitation spectra of $(R3HQ)_4RbEu(NO_3)_8$ measured at room temperature.

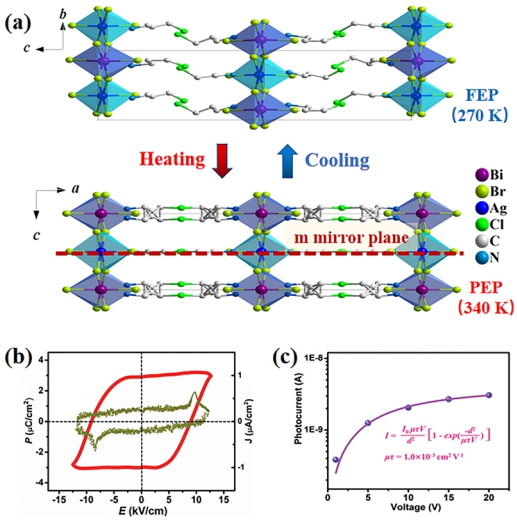

Figure 11. (a) Crystal structures of **12** at FEP (270 K) and PEP (340 K). (b) The *P-E* hysteresis loop and *J-E* curve measured at room temperature. (c) The *I-V* curve obtained under the X-ray irradiation.

MPA effects involving with its 2D quantum-confined motif. In combination of its ferroelectricity, this study provides a potential optically active ferroelectric candidate in the OHIPs family, which could be used in the broadband multiphoton applications.

n LEAD-FREE 2D PEROVSKITE-TYPE FERROELECTRICS

Compared with the developed lead-halogen perovskites, the lead-free counterparts have also attracted interests in term of environmental friendliness and sustainability. One of effective design strategies is element substitution of Pb to expand the family of halide double perovskites, namely, replacing two toxic Pb^{2+} in the crystal lattice using a couple of nontoxic heterovalent (*i.e.* monovalent and trivalent) metal cations. In particular, the formation of 2D double perovskites can accommodate large and flexible organic cations, such as quasi-spherical molecules and chiral organic ions, which are favorable to the emergence of phase transitions and ferroelectric orders. Regarding the advantages of both organic and inorganic components, the lead-free double perovskite ferroelectrics would hold potentials for diverse applications,[61] such as piezoelectric sensor, dielectric capacitor, nonlinear optical device and X-ray detection. In this section, we merely focus on the typical ferroelectric candidates of 2D double perovskites, including their structural phase transitions, ferroelectricity and photoelectric properties.

$(R3HQ)_4KCe(NO_3)_8$ (Compound 10) and $(R3HQ)_4RbEu(NO_3)_8$ (Compound 11). By using the low-symmetric chiral cations of R/S-3-hydroxylquinuclidinium (R3HQ and S3HQ), a series of polar 2D rare-earth double perovskites of $A_4M^IM^{III}(NO_3)_8$ have been recently synthesized by Ye. *et al*, and we here take the compound of $(R3HQ)_4KCe(NO_3)_8$ (**10**) as an example to discuss the structure-property relationship.[62] Compound **10** is a ferroelectric with the phase transition at T_c = 320 K. At low-temperature FEP, it belongs to a polar chiral space group $P2_1$ (symmetry elements: *E* and C_2). The inorganic frameworks formed by corner-sharing $K(NO_3)_6$ distorted octahedra and $Ce(NO_3)_6$ octahedra are alternatively arranged with organic R3HQ layers along the *c*-axis, thus forming 2D double perovskite motif. Half of the chiral organic cations are parallel to each other along the *b*-axis, while the other half are antiparallel to each other and perpendicular to the *b*-axis (Figure 10a). With the temperature exceeding beyond T_c, compound **10** undergoes phase transition and its structure changes to the nonpolar space group *B*222 (symmetry elements: *E*, C_2, $2C_2'$). Comparison of variable-temperature structures reveals that its phase transition is caused by the order-disordering of NO_3^- ions and organic cations. Symmetry breaking analyses confirm structural phase transition of **10** belongs to the Aizu nation of 222F2. As revealed by the *P-E* hysteresis loop and *J-E* curve, compound **10** has the P_s value of 4.1 μC·cm^{-2} (Figure 10b), solidly confirming its ferroelectric properties.

This family of 2D double perovskites not only shows room-temperature ferroelectric properties, but also enables tunable photoluminescent (PL) activity due to the rare-earth metals. For instance, the member of $(R3HQ)_4RbEu(NO_3)_8$ (compound **11**) exhibits strong PL emission with very high quantum yield. Owing to the homochirality of organic cations, the local symmetry environment of Eu^{3+} ion is disturbed. Thus, electric dipole transition $^5D_0 \rightarrow {}^7F_2$ is not absolutely forbidden and the environment of Eu^{3+} is not strictly symmetric, which are favorable to its PL emission (Figure 10c). The weak interactions between organic cations and Eu^{3+} ion might be used to tune PL properties.

$(CPA)_4AgBiBr_8$ (Compound 12). The lead-free double perovskites have also emerged as the potential candidates for detecting high-energy X-ray radiation. Recently, we have also presented a ferroelectric of 2D double perovskite, $(CPA)_4AgBiBr_8$ (CPA^+ = chloropropylammonium, **12**), which is sensitive to X-ray radiation.[63] At low-temperature phase (T_c = 305 K), it belongs to

DOI: 10.14102/j.cnki.0254-5861.2022-0013

the polar space group *Pc* (the point group *m*). The corner-sharing $AgBr_6$ distorted octahedra and $BiBr_6$ octahedra consist of inorganic frameworks, which alternate with organic CPA bilayers to form 2D monolayered structure of double perovskite. The directional alignment of organic CPA^+ cations with terminal halogen atoms make a significant contribution to the construction of polar structure (Figure 11a). At the high-temperature phase (above T_c), it crystallizes in the centrosymmetric space group *Pbam* (the point group *mmm*), and the organic CPA^+ cations become highly disordered with two kinds of molecular geometry. One is distributed over two equivalent orientations with respect to the crystallographic *m* mirror plane, while the other lies on the special symmetry plane. Along with the distortion decreasing of $AgBr_6$/$BiBr_6$ octahedra, the dipole moments cancel each other out and the bulk P_s disappears. This structural change corresponds to the symmetry breaking of **12** with an Aizu notation of *mmm*F*m*. The measured *P-E* hysteresis loop and *J-E* curve afford the P_s value of ~3.1 $\mu C \cdot cm^{-2}$ for **12** (Figure 11b), which is comparable with other 2D double perovskite ferroelectrics.

Interestingly, compound **12** is a semiconductor with the band gap of 2.69 eV. Its 2D layered structure allows efficient separation of excitons into free carriers due to the exposed layer edges.[64,65] These characteristics suggest the potentials of **12** for high-energy X-ray detection. Under X-ray irradiation, the photocurrent generated under the bias of 10 V is proportional to the dose rate. The slope for this linear fitting determines the sensitivity of X-ray detection is 0.8 $\mu C Gy_{air}^{-1} \cdot cm^{-2}$. Besides, alternating array of organic cation and inorganic perovskite sheets, like quantum-confined motif, endows a large mobility-lifetime product ($\mu\tau$ = 1.0×10^{-3} $cm^2 \cdot V^{-1}$) (Figure 11c). All these results reveal the potentials of **12** for X-ray detection and pave a way for exploring 2D double perovskite ferroelectrics with multifunctional properties.

n SUMMARY AND PROSPECT

In this minireview, we have presented recent advances of ferroelectric materials in the family of 2D hybrid perovskites. Structural origin for generating ferroelectricity is analyzed from the aspect of symmetry breaking. It is emphasized that the combination of ferroelectric polarizations with other semiconducting activities gives rise to new optoelectronic properties, which might create a class of ferroelectric semiconductors toward new photoelectronic applications. Up to date, the rational design of new candidates of ferroelectric semiconductors mainly depends on continuous experiments and partial accumulation of experience. How to predict and achieve the ferroelectric-type symmetry breaking is still challenging. Although great efforts have devoted to exploiting new ferroelectric semiconductors, the target-guided optimization of their performances is highly urgent for device applications. As exemplified by P_s-induced bulk ferroelectric photovoltaic effects, one of the most fascinating advantages is the achievement of above-bandgap photovoltages, while the relatively low photocurrent density and conversion efficiency restrict their practical solar-energy generation. Further, more attention should be paid to the coupling between other photo-induced properties and ferroelectric polarization. This is important to realize the new concepts of photoactive properties, such as the combination of photovoltaic and piezoelectric effects (*i.e.*, photostriction). As a multidisciplinary subject involving with chemistry, physics, crystallography and material science, the search for new candidate systems, which are in crystal/ceramic form, thin films or domain-engineered materials, is crucial for deep understanding on photoinduced activities in ferroelectric semiconductors or more generally polar materials. Probably, beyond the tip of iceberg in terms of P_s-induced bulk photovoltaic effects, it is necessary to establish a broad family of new ferroelectric semiconductors that we should exert our endeavors in future.

n ACKNOWLEDGEMENTS

This work is financially supported by National Natural Science Foundation of China (22125110, 21875251 and 21833010), the Key Research Program of Frontier Sciences of the Chinese Academy of Sciences (ZDBS-LY-SLH024), Fujian Science & Technology Innovation Laboratory for Optoelectronic Information of China (2021ZR126), the Strategic Priority Research Program of the CAS (XDB20010200) and Youth Innovation Promotion of CAS (Y201851).

n AUTHOR CONTRIBUTION

Yaoyao Chen and Changhao Gao contribute equally to this work.

n AUTHOR INFORMATION

Corresponding author. Email: sunzhihua@fjirsm.ac.cn (Z.H. Sun).

n COMPETING INTERESTS

The authors declare no competing interests.

n ADDITIONAL INFORMATION

Full paper can be accessed via
http://manu30.magtech.com.cn/jghx/EN/10.14102/j.cnki.0254-5861.2022-0013
For submission: https://mc03.manuscriptcentral.com/cjsc

REFERENCES

(1) Sun, Z. H.; Yi, X. F.; Tao, K. W.; Ji, C. M.; Liu, X. T.; Li, L. N.; Han, S. G.; Zheng, A. M.; Hong, M. C.; Luo, J. H. A molecular ferroelectric showing room-temperature record-fast switching of spontaneous polarization. *Angew. Chem. Int. Ed.* **2018**, 57, 9833–9837.

(2) Pandey, R.; Vats, G.; Yun, J.; Bowen, C. R.; Ho-Baillie, A. W. Y.; Seidel, J.; Butler, K. T.; Seok, S. I. Mutual insight on ferroelectrics and hybrid halide perovskites: a platform for future multifunctional energy conversion. *Adv. Mater.* **2019**, 31, 1807376.

(3) You, Y. M.; Liao, W. Q.; Zhao, D. W.; Ye, H. Y.; Zhang, Y.; Zhou, Q. H.; Niu, X. H.; Wang, J. L.; Li, P. F.; Fu, D. W.; Wang, Z. M.; Gao, S.; Yang, K. L.; Liu, J. M.; Li, J. Y.; Yan, Y. F.; Xiong, R. G. An organic-inorganic perovskite ferroelectric with large piezoelectric response. *Science* **2017**, 357, 306–309.

(4) Scott, J. F. Applications of modern ferroelectrics. *Science* **2007**, 315, 954–959.

(5) Scott, J. F. *Ferroelectric Memories Springer-Verlag*. Berlin **2000**.

(6) Ye, Z. G. *Handbook of Advanced Dielectric, Piezoelectric and Ferro-*

electric Materials: Synthesis, Properties and Applications. Elsevier **2008**.
(7) Spaldin, N. A.; Fiebig, M.; Mostovoy, M. The toroidal moment in condensed-matter physics and its relation to the magnetoelectric effect. *J. Phys.: Condens. Matter.* **2008**, 20, 434203.
(8) Litvin, D. B. Ferroic classifications extended to ferrotoroidic crystals. *Acta Crystallogr. Sect. A: Found. Crystallogr.* **2008**, 64, 316–320.
(9) Lee, J. H.; Fang, L.; Vlahos, E.; Ke, X.; Jung, Y. W.; Kourkoutis, L. F.; Kim, J. W.; Ryan, P. J.; Heeg, T.; Roeckerath, M.; Goian, V.; Bernhagen, M.; Uecker, R.; Hammel, P. C.; Rabe, K. M.; Kamba, S.; Schubert, J.; Freeland, J. W.; Muller, D. A.; Fennie, C. J.; Schiffer, P.; Gopalan, V.; Johnston-Halperin, E.; Schlom, D. G. A strong ferroelectric ferromagnet created by means of spin-lattice coupling. *Nature* **2010**, 466, 954–958.
(10) Horiuchi, S.; Tokura, Y. Organic ferroelectrics. *Nat. Mater.* **2008**, 7, 357–366.
(11) Hu, P. F.; Hu, S. B.; Huang, Y. D.; Reimers, J. R.; Rappe, A. M.; Li, Y. L.; Stroppa, A.; Ren, W. Bioferroelectric properties of glycine crystals. *J. Phys. Chem. Lett.* **2019**, 10, 1319–1324.
(12) Fu, D. W.; Zhang, W.; Cai, H. L.; Ge, J. Z.; Zhang, Y.; Xiong, R. G. Diisopropylammonium chloride: a ferroelectric organic salt with a high phase transition temperature and practical utilization level of spontaneous polarization. *Adv. Mater.* **2011**, 23, 201102938.
(13) Valasek, J. Piezo-electric and allied phenomena in Rochelle salt. *Phys. Rev.* **1921**, 17, 475–481.
(14) Han, S. G.; Li, M. F.; Liu, Y.; Guo, W. Q.; Hong, M. C.; Sun, Z. H.; Luo, J. H. Tailoring of a visible-light-absorbing biaxial ferroelectric towards broadband self-driven photodetection. *Nat. Commun.* **2021**, 12, 284.
(15) Fu, D. W.; Cai, H. L.; Liu, Y. M.; Ye, Q.; Zhang, W.; Zhang, Y.; Chen, X. Y.; Giovannetti, G.; Capone, M.; Li, J. Y.; Xiong, R. G. Diisopropylammonium bromide is a high-temperature molecular ferroelectric crystal. *Science* **2013**, 339, 425–428.
(16) Ye, H. Y.; Tang, Y. Y.; Li, P. F.; Liao, W. Q.; Gao, J. X.; Hua, X. N.; Cai, H.; Shi, P. P.; You, Y. M.; Xiong, R. G. Metal-free three-dimensional perovskite ferroelectrics. *Science* **2018**, 361, 151–155.
(17) Xu, H. J.; Guo, W. Q.; Wang, J. Q.; Ma, Y.; Han, S. G.; Liu, Y.; Lu, L.; Pan, X.; Luo, J. H.; Sun, Z. H. A metal-free molecular antiferroelectric material showing high phase transition temperatures and large electrocaloric effects. *J. Am. Chem. Soc.* **2021**, 143, 14379–14385.
(18) Kundys, B.; Lappas, A.; Viret, M.; Kapustianyk, V.; Rudyk, V.; Semak, S.; Simon, C.; Bakaimi, I. Multiferroicity and hydrogen-bond ordering in $(C_2H_5NH_3)_2CuCl_4$ featuring dominant ferromagnetic interactions. *Phys. Rev. B* **2010**, 81, 224434.
(19) Li, L. N.; Liu, X. T.; Li, Y. B.; Xu, Z.; Wu, Z. Y.; Han, S. G.; Tao, K. W.; Hong, M. C.; Luo, J. H.; Sun, Z. H. Two-dimensional hybrid perovskite-type ferroelectric for highly polarization-sensitive shortwave photodetection. *J. Am. Chem. Soc.* **2019**, 141, 2623–2629.
(20) Ma, Y.; Wang, J. Q.; Guo, W. Q.; Han, S. G.; Xu, J. L.; Liu, Y.; Lu, L.; Xie, Z. D.; Luo, J. H.; Sun, Z. H. The first improper ferroelectric of 2D multilayered hybrid perovskite enabling strong tunable polarization-directed second harmonic generation effect. *Adv. Fun. Mater.* **2021**, 31, 2103012.
(21) Liu, H. Y.; Zhang, H. Y.; Chen, X. G.; Xiong, R. G. Molecular design principles for ferroelectrics: ferroelectrochemistry. *J. Am. Chem. Soc.* **2020**, 142, 15205–15218.
(22) Cohen, R. E. Origin of ferroelectricity in perovskite oxides. *Nature* **1992**, 358, 136–138.
(23) Fu, H. X.; Cohen, R. E. Polarization rotation mechanism for ultrahigh electromechanical response in single-crystal piezoelectrics. *Nature* **2000**, 403, 281–283.
(24) Saha, S.; Sinha, T. P.; Mookerjee, A. Electronic structure, chemical bonding, and optical properties of paraelectric $BaTiO_3$. *Phys. Rev. B* **2000**, 62, 8828–8834.
(25) Levin, I.; Tucker, M. C.; Wu, H.; Provenzano, V.; Dennis, C. L.; Karimi, S.; Comyn, T.; Stevenson, T.; Smith, R. I.; Reaney, I. M. Displacive phase transitions and magnetic structures in Nd-substituted $BiFeO_3$. *Chem. Mater.* **2011**, 23, 2166–2175.
(26) Shi, P. P.; Tang, Y. Y.; Li, P. F.; Liao, W. Q.; Wang, Z. X.; Ye, Q.; Xiong, R. G. Symmetry breaking in molecular ferroelectrics. *Chem. Soc. Rev.* **2016**, 45, 3811–3827.
(27) Zhang, W.; Xiong, R. G. Ferroelectric metal-organic frameworks. *Chem. Rev.* **2012**, 112, 1163–1195.
(28) Xu, G. C.; Ma, X. M.; Zhang, L.; Wang, Z. M.; Gao, S. Disorder-order ferroelectric transition in the metal formate framework of $[NH_4][Zn(HCOO)_3]$. *J. Am. Chem. Soc.* **2010**, 132, 9588–9590.
(29) Xu, G. C.; Zhang, W.; Ma, X. M.; Chen, Y. H.; Zhang, L.; Cai, H. L.; Wang, Z. M.; Xiong, R. G.; Gao, S. Coexistence of magnetic and electric orderings in the metal-formate frameworks of $[NH_4][M(HCOO)_3]$. *J. Am. Chem. Soc.* **2011**, 133, 14948–14951.
(30) Xu, H. J.; Han, S. G.; Sun, Z. H.; Luo, J. H. Recent advances of two-dimensional organic-inorganic hybrid perovskite ferroelectric materials. *Acta Chim. Sin.* **2021**, 79, 23–35.
(31) Wang, Y. N.; Huang, J. W.; Wang, L.; She, H. D.; Wang, Q. Z. Research progress of ferrite materials for photoelectrochemical water splitting. *Chin. J. Struct. Chem.* **2022**, 41, 2201054–2201068.
(32) Ji, C. M.; Li, Y. Z.; Liu, X. T.; Wang, Y. X.; Zhu, T. T.; Chen, Q.; Li, L. N.; Wang, S. A.; Luo, J. H. Monolayer-to-multilayer dimensionality reconstruction in a hybrid perovskite for exploring the bulk photovoltaic effect enables passive X-ray detection. *Angew. Chem. Int. Ed.* **2021**, 60, 20970–20976.
(33) Li, M. F.; Han, S. G.; Liu, Y.; Luo, J. H.; Hong, M. C.; Sun, Z. H. Soft perovskite-type antiferroelectric with giant electrocaloric strength near room temperature. *J. Am. Chem. Soc.* **2020**, 142, 20744–20751.
(34) Han, S. G.; Wang, G. E.; Xu, G.; Luo, J. H.; Sun, Z. H. Ferroelectric perovskite-type films with robust in-plane polarization toward efficient room-temperature chemiresistive sensing. *Fundam. Res.* **2022**, doi: 10.1016/j.fmre.2022.01.015.
(35) Zhang, H.; Chen, X.; Tang, Y.; Liao, W.; Di, F.; Mu, X.; Peng, H.; Xiong, R. PFM (piezoresponse force microscopy)-aided design for molecular ferroelectrics. *Chem. Soc. Rev.* **2021**, 50, 8248–8278.
(36) You, Y. M.; Tang, Y. Y.; Li, P. F.; Zhang, H. Y.; Zhang, W. Y.; Zhang, Y.; Ye, H. Y.; Nakamura, T.; Xiong, R. G. Quinuclidinium salt ferroelectric thin-film with duodecuple-rotational polarization-directions. *Nat. Commun.* **2017**, 8, 14934.
(37) Tang, Y. Y.; Xie, Y. F.; Zeng, Y. L.; Liu, J. C.; He, W. H.; Huang, X. Q.; Xiong, R. G. Record enhancement of phase transition temperature realized by H/F substitution. *Adv. Mater.* **2020**, 32, 2003530.
(38) Ji, C. M.; Wang, S.; Li, L. N.; Sun, Z. H.; Hong, M. C.; Luo, J. H. The first 2D hybrid perovskite ferroelectric showing broadband white-light emission with high color rendering index. *Adv. Fun. Mater.* **2018**, 29, 1805038.
(39) Cortecchia, D.; Yin, J.; Bruno, A.; Lo, S. A.; Gurzadyan, G. G.; Mhaisalkar, S.; Brédas, J.; Soci, C. Polaron self-localization in white-light emitting hybrid perovskites. *J. Mater. Chem. C* **2017**, 5, 2771–2780.

DOI: 10.14102/j.cnki.0254-5861.2022-0013

(40) Sha, T. T.; Xiong, Y. A.; Pan, Q.; Chen, X. G.; Song, X. J.; Yao, J.; Miao, S. R.; Jing, Z. Y.; Feng, Z. J.; You, Y. M.; Xiong, R. G. Fluorinated 2D lead iodide perovskite ferroelectrics. *Adv. Mater.* **2019**.

(41) Aizu, K. Possible species of "ferroelastic" crystals and of simultaneously ferroelectric and ferroelastic crystals. *J. Phys. Soc. Jpn.* **1969**, 27, 387–396.

(42) Aizu, K. Possible species of ferromagnetic, ferroelectric, and ferroelastic crystals. *Phys. Rev. B* **1970**, 2, 754–772.

(43) Ji, C. M.; Dey, D.; Peng, Y.; Liu, X. T.; Li, L. N.; Luo, J. H. Ferroelectricity-driven self-powered ultraviolet photodetection with strong polarization sensitivity in a two-dimensional halide hybrid perovskite. *Angew. Chem. Int. Ed.* **2020**, 59, 18933–18937.

(44) Huang, P. J.; Taniguchi, K.; Miyasaka, H. Bulk photovoltaic effect in a pair of chiral-polar layered perovskite-type lead iodides altered by chirality of organic cations. *J. Am. Chem. Soc.* **2019**, 141, 14520–14523.

(45) Ji, W.; Yao, K.; Liang, Y. C. Bulk photovoltaic effect at visible wavelength in epitaxial ferroelectric $BiFeO_3$ thin films. *Adv. Mater.* **2010**, 22, 1763–1766.

(46) Yang, S. Y.; Seidel, J.; Byrnes, S. J.; Shafer, P.; Yang, C. H.; Rossell, M. D.; Yu, P.; Chu, Y. H.; Scott, J. F.; Ager, J. W., 3rd; Martin, L. W.; Ramesh, R. Above-bandgap voltages from ferroelectric photovoltaic devices. *Nat. Nanotechnol.* **2010**, 5, 143–147.

(47) Li, L. N.; Sun, Z. H.; Wang, P.; Hu, W. D.; Wang, S. S.; Ji, C. M.; Hong, M. C.; Luo, J. H. Tailored engineering of an unusual $(C_4H_9NH_3)_2(CH_3NH_3)_2Pb_3Br_{10}$ two-dimensional multilayered perovskite ferroelectric for a high-performance photodetector. *Angew. Chem. Int. Ed.* **2017**, 56, 12150–12154.

(48) Li, L. N.; Shang, X. Y.; Wang, S. S.; Dong, N. N.; Ji, C. M.; Chen, X. Y.; Zhao, S. G.; Wang, J.; Sun, Z. H.; Hong, M. C.; Luo, J. H. Bilayered hybrid perovskite ferroelectric with giant two-photon absorption. *J. Am. Chem. Soc.* **2018**, 140, 6806–6809.

(49) Zhang, R.; Fan, J. D.; Zhang, X.; Yu, H. H.; Zhang, H. J.; Mai, Y. H.; Xu, T. X.; Wang, J. Y.; Snaith, H. J. Nonlinear optical response of organic-inorganic halide perovskites. *ACS Photonics* **2016**, 3, 371–377.

(50) Wang, J. Q.; Liu, Y.; Han, S. G.; Ma, Y.; Li, Y. B.; Xu, Z. Y.; Luo, J. H.; Hong, M. C.; Sun, Z. H. Ultrasensitive polarized-light photodetectors based on 2D hybrid perovskite ferroelectric crystals with a low detection limit. *Sci. Bull.* **2021**, 66, 158–163.

(51) Wu, Z. Y.; Ji, C. M.; Li, L. N.; Kong, J. T.; Sun, Z. H.; Zhao, S. G.; Wang, S. S.; Hong, M. C.; Luo, J. H. Alloying n-butylamine into $CsPbBr_3$ to give a two-dimensional bilayered perovskite ferroelectric material. *Angew. Chem. Int. Ed.* **2018**, 57, 8140–8143.

(52) Liu, Y.; Pan, X.; Liu, X. T.; Han, S. G.; Wang, J. Q.; Lu, L.; Xu, H. J.; Sun, Z. H.; Luo, J. H. Tailoring interlayered spacers of 2D cesium-based perovskite ferroelectrics toward exceptional ferro-pyro-phototronic effects. *Small* **2021**, 2106888.

(53) Liu, Y.; Han, S. G.; Wang, J. Q.; Ma, Y.; Guo, W. Q.; Huang, X. Y.; Luo, J. H.; Hong, M. C.; Sun, Z. H. Spacer cation alloying of a homoconformational carboxylate trans isomer to boost in-plane ferroelectricity in a 2D hybrid perovskite. *J. Am. Chem. Soc.* **2021**, 143, 2130–2137.

(54) Wang, J.; Gudiksen, M. S.; Duan, X.; Cui, Y.; Lieber, C. M. Highly polarized photoluminescence and photodetection from single indium phosphide nanowires. *Science* **2001**, 293, 1455–1457.

(55) Peng, Y.; Liu, X. T.; Sun, Z. H.; Ji, C. M.; Li, L. N.; Wu, Z. Y.; Wang, S. S.; Yao, Y. P.; Hong, M. C.; Luo, J. H. Exploiting the bulk photovoltaic effect in a 2D trilayered hybrid ferroelectric for highly sensitive polarized light detection. *Angew. Chem. Int. Ed.* **2020**, 59, 3933–3937.

(56) Xu, Z. Y.; Weng, W.; Li, Y. B.; Liu, X. T.; Yang, T.; Li, M. F.; Huang, X. Y.; Luo, J. H.; Sun, Z. H. 3D-to-2D dimensional reduction for exploiting a multilayered perovskite ferroelectric toward polarized-light detection in the solar-blind ultraviolet region. *Angew. Chem. Int. Ed.* **2020**, 59, 21693–21697.

(57) Chen, H. Y.; Liu, K. W.; Hu, L. F.; Al-Ghamdi, A. A.; Fang, X. S. New concept ultraviolet photodetectors. *Mater. Today* **2015**, 18, 493–502.

(58) Xie, C.; Lu, X. T.; Tong, X. W.; Zhang, Z. X.; Liang, F. X.; Liang, L.; Luo, L. B.; Wu, Y. C. Recent progress in solar-blind deep-ultraviolet photodetectors based on inorganic ultrawide bandgap semiconductors. *Adv. Fun. Mater.* **2019**, 29,1806006.

(59) Sutherland, R. L. *Handbook of Nonlinear Optics*. CRC Press **2003**.

(60) Li, M. F.; Xu, Y. M.; Han, S. G.; Xu, J. L.; Xie, Z. D.; Liu, Y.; Xu, Z. Y.; Hong, M. C.; Luo, J. H.; Sun, Z. H. Giant and broadband multiphoton absorption nonlinearities of a 2D organometallic perovskite ferroelectric. *Adv. Mater.* **2020**, 32, 2002972.

(61) Nicolo, F.; Plancherel, D.; Chapuis, G.; Buenzli, J. C. G. Complexes of lanthanoid salts with macrocyclic ligands. 34. Glasslike structure in crystalline macrocyclic complexes: synthesis, X-ray diffraction, and laser-spectroscopic investigation of neodymium(III) and europium(III) complexes with 4,13-dimethyl-1,7,10,16-tetraoxa-4,13-diazacyclooctadecane. *Inorg. Chem.* **1988**, 27, 3518–3526.

(62) Shi, C.; Ye, L.; Gong, Z. X.; Ma, J. J.; Wang, Q. W.; Jiang, J. Y.; Hua, M. M.; Wang, C. F.; Yu, H.; Zhang, Y.; Ye, H. Y. Two-dimensional organic-inorganic hybrid rare-earth double perovskite ferroelectrics. *J. Am. Chem. Soc.* **2020**, 142, 545–551.

(63) Guo, W. Q.; Liu, X. T.; Han, S. G.; Liu, Y.; Xu, Z. Y.; Hong, M. C.; Luo, J. H.; Sun, Z. H. Room-temperature ferroelectric material composed of a two-dimensional metal halide double perovskite for X-ray detection. *Angew. Chem. Int. Ed.* **2020**, 59, 13879–13884.

(64) Tsai, H.; Nie, W.; Blancon, J. C.; Stoumpos, C. C.; Asadpour, R.; Harutyunyan, B.; Neukirch, A. J.; Verduzco, R.; Crochet, J. J.; Tretiak, S.; Pedesseau, L.; Even, J.; Alam, M. A.; Gupta, G.; Lou, J.; Ajayan, P. M.; Bedzyk, M. J.; Kanatzidis, M. G. High-efficiency two-dimensional Ruddlesden-Popper perovskite solar cells. *Nature* **2016**, 536, 312–316.

(65) Blancon, J. C.; Tsai, H.; Nie, W.; Stoumpos, C. C.; Pedesseau, L.; Katan, C.; Kepenekian, M.; Soe, C. M. M.; Appavoo, K.; Sfeir, M. Y.; Tretiak, S.; Ajayan, P. M.; Kanatzidis, M. G.; Even, J.; Crochet, J. J.; Mohite, A. D. Extremely efficient internal exciton dissociation through edge states in layered 2D perovskites. *Science* **2017**, 355, 1288–1292.

Received: January 19, 2022
Accepted: February 11, 2022
Published: April 8, 2022

DOI: 10.14102/j.cnki.0254-5861.2022-0013